Research Square

Preprints are preliminary reports that have not undergone peer review.
They should not be considered conclusive, used to inform clinical practice,
or referenced by the media as validated information.

A Proof-of-Concept Graphene-Functionalised Embroidered Textile Biosensing Platform for Salivary Alzheimer's Disease Biomarker Detection

Bethany Richardson

B.Richardson@derby.ac.uk

University of Derby

Alex Casson

University of Manchester

Christopher Blanford

University of Manchester

Urvashi Gunputh

University of Derby

Research Article

Keywords: Textile biosensors, Alzheimer’s Disease, Wearable diagnostics, biosensing platform

Posted Date: August 27th, 2026

DOI: https://doi.org/10.21203/rs.3.rs-10535881/v1

License: This work is licensed under a Creative Commons Attribution 4.0 International License.
Read Full License

Additional Declarations: No competing interests reported.

Manuscript Title:

A Proof-of-Concept Graphene-Functionalised Embroidered Textile Biosensing Platform for Salivary Alzheimer's Disease Biomarker Detection

Dr Bethany Richardson* [1,2] , Professor Alex Casson [2], Dr Christopher Blanford, Dr Urvashi Gunputh[1]

1 University of Derby, Derby, United Kingdom

2 University of Manchester, Manchester, United Kingdom

*Correspondence: B.Richardson@derby.ac.uk

Abstract

Electrochemical biosensors offer a promising route for the rapid, non-invasive detection of disease biomarkers by converting biochemical interactions into measurable electrical signals. Although Alzheimer's disease (AD) diagnosis currently relies primarily on blood and cerebrospinal fluid analyses, these approaches are invasive, costly, and unsuitable for continuous monitoring. Saliva has emerged as an attractive alternative biofluid due to its non-invasive collection and growing evidence supporting the presence of AD-associated biomarkers. In this study, a flexible textile-based biosensing platform was developed for the detection of AD biomarkers using embroidered interdigitated electrodes (IDEs) integrated within a multilayer fabric substrate. The IDEs were functionalised with graphene oxide (GO), reduced graphene oxide (rGO), anti-tau-functionalised GO (AntiTau-GO), and anti-tau-functionalised rGO (AntiTau-rGO) conductive inks. Surface chemistry was modified using EDC/NHS-mediated covalent immobilisation of anti-tau antibodies to further test the surface stability. The electrical stability and sensing performance of the embroidered biosensing platforms were evaluated using electrochemical resistance measurements following exposure to deionised water, phosphate-buffered saline, artificial saliva, tau protein, and amyloid-β (Aβ) protein. The rGO-coated electrodes demonstrated improved electrical stability and lower resistance variation compared with GO-coated electrodes, reflecting enhanced conductivity following chemical reduction. Furthermore, the AntiTau-rGO biosensing platforms exhibited the most stable functionalisation and measurable resistance responses following exposure to tau protein. This suggests feasibility of antibody-functionalised textile electrodes for selective biomarker detection with further development. These findings highlight the potential of graphene-functionalised embroidered biosensing platforms as low-cost, wearable platforms for the non-invasive monitoring of Alzheimer's disease biomarkers in saliva.

Keywords

Textile biosensors; Alzheimer’s Disease; Wearable diagnostics; biosensing platform

Funding Declaration
The authors received no funding for the research, authorship, and publication of this article.

Consent to participate Declaration
Consent to participate is not applicable.

Consent to publish Declaration
All authors involved in the making of this publication have provided consent for publication and distribution of work.

Competing interests
There are no competing interests from the Authors in the publication of this article.

Ethics Approval
This article does not contain any studies with human participants or animals performed by any of the authors. Therefore, ethics approval was not required for this research. All data was carried out in laboratory conditions.

Permission to use third-party material
Not applicable as no third-party material has been used.

Data Availability
The datasets generated and analysed during the current study are available in the Zenodo repository https://doi.org/10.5281/zenodo.19652122.

Acknowledgements
Thank you to Professor Alex Casson and Dr Christopher Blanford at the University of Manchester for their Supervision during this study. Prof. Casson assisted with project conceptualization, data analysis using Python and editing. Dr Blanford assisted with SEM, EDX imaging analysis. Thank you to Theo Cordeiro for formatting of data with use of MATLAB.

Author Contribution
BR wrote the main manuscript text, responsible for conceptualization and data curation. AC was the main Supervisor of the project alongside CB as second Supervisor. AC assisted with software coding, data visualization and reviewing and editing manuscript. CB provided software coding and data visualization. UG assisted with reviewing and editing manuscript.

1. Introduction

Alzheimer's disease (AD) is the most common cause of dementia, accounting for approximately 60–70% of all dementia cases worldwide, with prevalence expected to increase substantially due to an ageing global population [1]. Characterised by progressive neuronal degeneration and

cognitive decline, AD places a significant burden on healthcare systems and remains one of the leading causes of disability and mortality among older adults [2]. Early diagnosis is increasingly recognised as essential for improving patient outcomes, enabling earlier therapeutic intervention, disease monitoring, and recruitment into clinical trials investigating disease-modifying therapies [3]. The pathological hallmarks of AD include the extracellular accumulation of amyloid-β (Aβ) peptides and the intracellular aggregation of hyperphosphorylated tau proteins into neurofibrillary tangles [4]. These biomarkers form the basis of the AT(N) research framework proposed by the National Institute on Aging and Alzheimer's Association (NIA-AA), which classifies AD according to amyloid deposition (A), tau pathology (T), and neurodegeneration (N) rather than clinical symptoms alone [5]. Consequently, accurate quantification of Aβ and tau proteins has become central to contemporary AD diagnosis and disease staging.

Recent advances in biomarker analysis have transformed AD diagnostics. Cerebrospinal fluid (CSF) assays and positron emission tomography (PET) imaging remain the clinical gold standards but are expensive, require specialised facilities, and involve invasive lumbar puncture or exposure to radioactive tracers [6]. More recently, blood-based biomarker assays have demonstrated excellent diagnostic performance, particularly phosphorylated tau (pTau217), pTau181 and plasma Aβ42/Aβ40 ratios [7]. These developments culminated in the U.S. Food and Drug Administration (FDA) clearance of the Lumipulse® G pTau217/β-Amyloid 1-42 Plasma Ratio assay in 2025, representing the first FDA-cleared blood test to aid the diagnosis of Alzheimer's disease [8]. Despite these significant advances, blood-based diagnostics still require venepuncture, laboratory processing and trained personnel, limiting their suitability for continuous monitoring and home-based healthcare.

Saliva has emerged as an attractive alternative biofluid for AD diagnostics because it can be collected rapidly, repeatedly and non-invasively without requiring trained clinicians [9]. Several studies have demonstrated measurable concentrations of Aβ peptides and tau proteins in saliva, suggesting that salivary biomarkers may provide a practical route towards point-of-care Alzheimer's disease screening [10]. However, salivary biomarker concentrations are considerably lower than those found in blood or CSF, necessitating highly sensitive biosensing platforms capable of selective detection within complex biological matrices [11]. Electrochemical biosensors have attracted considerable attention as promising analytical platforms because they convert biochemical recognition events into measurable electrical signals while offering high sensitivity, rapid response times, low sample volumes and compatibility with portable instrumentation [12]. Graphene-based nanomaterials have become particularly attractive for electrochemical biosensing owing to their exceptional electrical conductivity, large specific surface area, mechanical flexibility and ease of chemical functionalisation [13], [14]. Graphene oxide (GO) contains abundant oxygen-containing functional groups, including hydroxyl, epoxy and carboxyl groups, which facilitate covalent immobilisation of biomolecules through established coupling chemistries such as EDC/NHS [15]. Chemical reduction of GO to reduced graphene oxide (rGO) partially restores the sp^2 carbon network, significantly improving electrical conductivity while retaining sufficient functional groups for antibody attachment [16]. Numerous graphene-based electrochemical biosensors have recently been reported for Alzheimer's disease biomarker detection, including field-effect transistor sensors, screen-printed electrodes, laser-induced graphene electrodes and microfabricated interdigitated electrode (IDE) platforms capable of detecting tau proteins or Aβ at picomolar concentrations [12], [17], [18]. Although these sensors demonstrate excellent analytical performance, they are predominantly fabricated on rigid silicon, glass or polymer substrates using conventional microfabrication techniques, which can increase manufacturing cost and limit their integration into wearable healthcare technologies. Furthermore, relatively few studies have investigated biosensors specifically designed for non-invasive salivary biomarker detection using flexible textile substrates.

Textile-based biosensors represent an emerging class of wearable diagnostic devices that combine flexibility, breathability and user comfort with low-cost manufacturing and large-area

fabrication [19]. Conductive yarns can be embroidered directly into fabrics to produce complex electrode geometries without conventional lithographic processes, enabling scalable manufacturing of wearable electrochemical sensors. The incorporation of graphene-based conductive coatings further enhances sensor conductivity while providing chemically active surfaces suitable for biomolecule immobilisation [20]. Despite these advantages, embroidered textile biosensors have received little attention for Alzheimer's disease diagnostics, particularly for antibody-functionalised detection of tau biomarkers. Table 1 compares representative graphene-based Alzheimer's disease biosensors with the embroidered textile platform developed in the present study. Most reported devices employ rigid silicon, glass, or screen-printed substrates fabricated using conventional microfabrication techniques. While these platforms demonstrate excellent analytical sensitivity, they are generally not designed for integration into wearable textiles. In contrast, the present work combines embroidered silver-coated interdigitated electrodes, graphene-based nanomaterials, EDC/NHS antibody immobilisation and a multilayer textile architecture within a saliva-compatible sensing platform. Although this study represents a proof-of-concept demonstration rather than a fully validated analytical device, the platform establishes a foundation for future wearable, non-invasive monitoring of Alzheimer's disease biomarkers.

Table 1. Comparison of recently reported Alzheimer's disease biosensors with the proposed embroidered textile biosensing platform

Study	Substrate	Sensing Material	Target Biomarker	Detection Method	Key Advantages	Limitations
Zhao et al. (2024)	Silicon FET	Graphene	Tau, Aβ	Field-effect transistor	Ultra-high sensitivity, rapid response	Rigid substrate, complex microfabrication, unsuitable for wearable applications
Shahdeo et al. (2022)	Gold electrode	Gold nanorods	Protein biomarkers	Electrochemical immunosensor	High analytical sensitivity	Rigid platform requiring laboratory instrumentation
Chudziak et al. (2023)	Planar electrode	Reduced graphene oxide	General electrochemical sensing	Resistance/Electrochemical	High conductivity following reduction	Not designed for wearable biosensing or Alzheimer's detection
Recent screen-printed graphene biosensors	Screen-printed polymer	Graphene/rGO	Tau or Aβ	Electrochemical impedance/voltammetry	Disposable, good sensitivity	Limited flexibility; not suitable for integration into textiles
This work	Embroidered multilayer textile	GO, rGO and AntiTau-rGO	Tau (proof-of-concept) and Aβ	Two-wire resistance monitoring	Flexible embroidered electrodes, saliva-compatible sensing,	Proof-of-concept study; calibration curves, LOD, LOQ, larger sample size,

Study	Substrate	Sensing Material	Target Biomarker	Detection Method	Key Advantages	Limitations
					wearable textile platform, inexpensive fabrication, graphene functionalisation with covalent antibody immobilisation	EIS validation and clinical testing remain future work

In this work, a proof-of-concept is explored for the development of a flexible embroidered textile biosensing platform for detection of Alzheimer's disease biomarkers. In this work, silver-coated embroidered interdigitated electrodes were integrated into a multilayer textile substrate. This was functionalised using graphene oxide (GO), reduced graphene oxide (rGO), anti-tau-functionalised GO (AntiTau-GO) and anti-tau-functionalised rGO (AntiTau-rGO) conductive coatings. Anti-tau antibodies were covalently immobilised using EDC/NHS coupling chemistry to deposit the antibodies onto the sensors surface [21]. The electrical stability of the embroidered sensors was evaluated following exposure to deionised water, phosphate-buffered saline (PBS), artificial saliva, Aβ and tau protein using electrochemical resistance measurement. The proposed platform combines embroidered conductive textiles, graphene nanomaterials, antibody functionalisation and saliva-compatible sensing within a single wearable biosensor, providing a novel approach towards low-cost, non-invasive monitoring of Alzheimer's disease biomarkers.

2. Materials and Methods

2.1 Fabric Substrate

A multilayer textile substrate was used to construct the biosensing platform shown in Figure 1. The fabric substrates were chosen as it is commonly used in medical textiles due to their hydrophilic and hydrophobic properties. A multilayer textile substrate was developed to provide mechanical support and controlled fluid transport for the embroidered biosensing platform (Fig. 1a). The substrate comprised three functional layers designed to facilitate analyte delivery while maintaining electrical isolation and structural integrity. The upper sensing layer consisted of 100% woven cotton fabric, selected for its hydrophilic nature, high absorbency and compatibility with graphene-based conductive inks. The porous fibre structure promotes uniform adsorption and retention of the graphene oxide (GO) and reduced graphene oxide (rGO) inks, providing a stable conductive coating following drying. The conductive coatings were prepared from aqueous GO and rGO dispersions at concentrations of 0.5 mg mL^{-1} and 1.0 mg mL^{-1}, respectively. The inks were deposited onto the embroidered interdigitated electrode (IDE) region using a calibrated micropipette before drying at room temperature to produce a uniform conductive sensing layer. A nonwoven medical-grade gauze layer was positioned beneath the sensing layer to absorb excess sample volume, minimise lateral liquid spreading and promote consistent diffusion of the analyte towards the

sensing region [22]. The bottom layer consisted of a hydrophobic polyester-based medical textile, which acted as a liquid barrier to prevent sample leakage and provide mechanical stability during handling. The combination of hydrophilic and hydrophobic textile layers enabled controlled sample transport while maintaining flexibility, making the platform suitable for wearable biosensing applications.

2.2 Embroidered Electrodes

Interdigitated electrodes (IDEs) were fabricated by computer-controlled embroidery using a ZSK industrial embroidery machine (ZSK Stickmaschinen GmbH, Germany)**.** The electrode pattern was embroidered directly onto the cotton sensing layer using a silver-coated polyamide conductive embroidery thread (Madeira HC 12, Madeira Garnfabrik, Germany), selected for its low electrical resistance (approximately <300 Ω m^{-1}), high flexibility and compatibility with textile manufacturing processes. The IDE geometry comprised two interlocking comb-shaped electrodes connected to square contact pads for electrical interrogation (Fig. 1b). This configuration increases the effective sensing area while producing a highly non-uniform electric field between adjacent electrode fingers, thereby enhancing sensitivity to changes in dielectric properties occurring at the electrode surface during biomolecular interactions. The embroidered conductive thread also provided excellent mechanical robustness, allowing the electrodes to withstand repeated bending and deformation without significant degradation in electrical performance. Following embroidery, graphene-based conductive inks were deposited over the IDE sensing region to reduce the intrinsic resistance of the conductive thread and provide a nanostructured surface rich in oxygen-containing functional groups for subsequent antibody immobilisation using EDC/NHS chemistry.

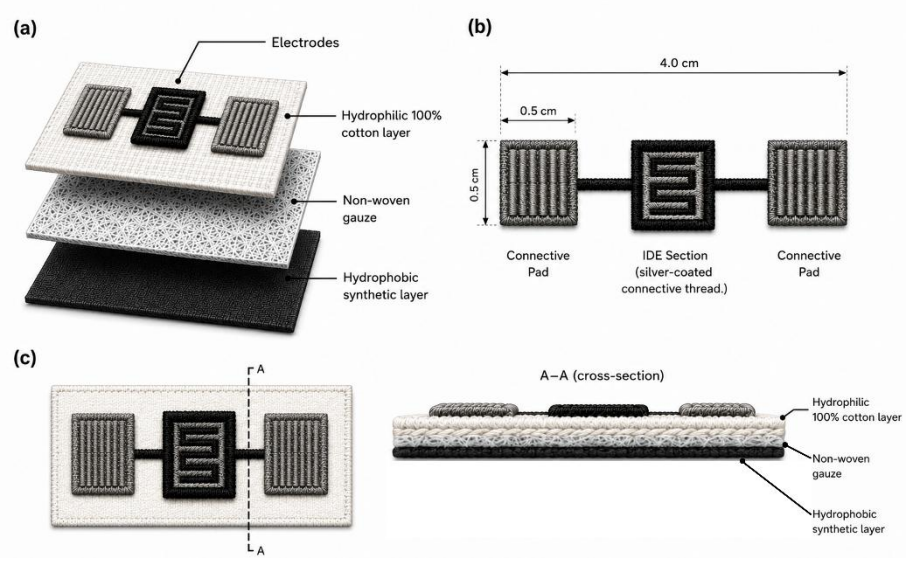


Fig 1. a) Textile-based sensing platform expanded view of fabric layers with embroidery on surface b) Isolated view of embroidered sensor from sensing platform surface c) Cross-section of fabric layers of sensing platform

2.3 Graphene Oxide and reduced Graphene Oxide Synthesis

Graphene oxide was synthesised using a modified Hummers method (Fig 2). Graphene oxide (GO) is widely employed in electrochemical biosensing owing to its ease of processing and the abundance of oxygen-containing functional groups (OFGs), including

hydroxyl, epoxy, carbonyl, and carboxyl groups, which facilitate subsequent chemical functionalisation [13]. These functional groups also provide GO with excellent dispersibility in aqueous media, making it an attractive precursor for conductive graphene-based materials. Following chemical reduction, the partial restoration of the sp^2 carbon network significantly improves the electrical conductivity and electron mobility while retaining sufficient functional groups for biomolecule immobilisation [23]. GO was synthesised using a modified Hummers method adapted from Marcano *et al.* [16]. Initially, 0.5 g of expandable graphite flakes was thermally exfoliated in a 750 W microwave oven for 20 s. The expanded graphite was immediately transferred into 100 mL of concentrated sulphuric acid (98 wt%) under continuous stirring, after which 5 g of potassium permanganate ($KMnO_4$) was gradually added while maintaining the reaction temperature below 20 °C. The oxidation reaction was allowed to proceed for 24 h under continuous stirring.

Following oxidation, the reaction was terminated by slowly adding hydrogen peroxide (H_2O_2) to the reaction mixture while immersed in an ice bath. The solution colour changed from dark purple to bright yellow, confirming the reduction of residual permanganate ions and completion of the oxidation process. The resulting GO suspension was repeatedly washed by centrifugation at 1500 × g for 20 min, followed by replacement of the supernatant with deionised (DI) water. This washing procedure was repeated five times until a near-neutral pH was obtained, removing residual acids and manganese-containing by-products. The purified GO was then dispersed in DI water by ultrasonication for 30 min to obtain a homogeneous stock dispersion. The GO concentration was determined gravimetrically by drying a known volume of dispersion and calculating the dry mass. From this stock solution, GO inks with concentrations of 0.5 mg mL^{-1} and 1.0 mg mL^{-1} were prepared by dilution or concentration with DI water. Reduced graphene oxide (rGO) ink was subsequently prepared via chemical reduction of the GO dispersion using L-ascorbic acid (0.10 M) as an environmentally benign reducing agent. L-ascorbic acid was added to the GO dispersion under continuous magnetic stirring and the mixture was heated to 95 °C for 1 h, promoting the removal of oxygen-containing functional groups and partial restoration of the conjugated graphene structure. The reduced dispersion was allowed to cool to room temperature before being centrifuged and washed with DI water to remove residual reducing agent and reaction by-products. The resulting rGO ink was finally redispersed by ultrasonication to produce a stable conductive ink suitable for coating the embroidered interdigitated electrode (IDE) sensors.

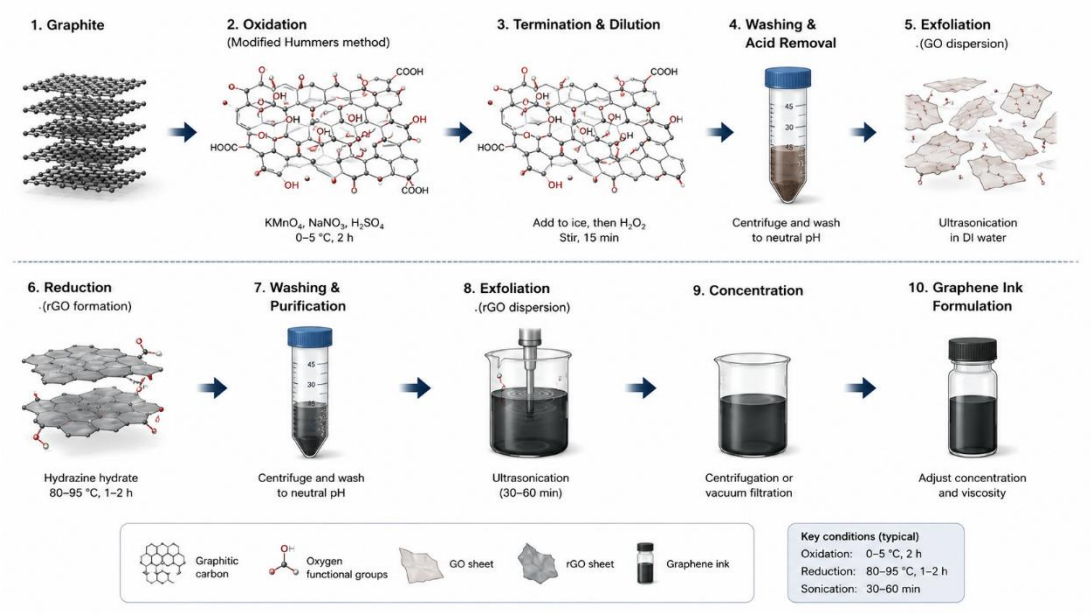


Fig 2. Modified Hummer's method process for synthesis of graphene ink

2.4 AntiTau Surface Functionalisation

Anti-tau antibodies were covalently immobilised onto the reduced graphene oxide (rGO)-coated interdigitated electrode (IDE) sensors using carbodiimide (EDC/NHS) coupling chemistry. This approach activates carboxyl groups present on the rGO surface, enabling stable amide bond formation with primary amine groups on antibody molecules and producing a robust biofunctional sensing interface [15], [24]. The immobilisation reagents were obtained from Sigma-Aldrich (UK), including 2-(N-morpholino)ethanesulfonic acid (MES) buffer (5 mmol L^{-1}, pH 4.0), 1-ethyl-3-(3-dimethylaminopropyl)carbodiimide hydrochloride (EDC), N-hydroxysuccinimide (NHS), phosphate-buffered saline (PBS, 20 mmol L^{-1}, pH 7.4), and 2% (w/v) bovine serum albumin (BSA). Mouse monoclonal anti-tau antibodies and recombinant Tau-441 (P301S) protein were also purchased from Sigma-Aldrich. Initially, 1 mg of rGO was dispersed in 5 mmol L^{-1} MES buffer (pH 4.0) by ultrasonication to obtain a homogeneous suspension. Surface carboxyl groups were activated by adding EDC (4 mg mL^{-1}) and NHS (6 mg mL^{-1}) to the dispersion. The reaction mixture was maintained under continuous stirring at 10 °C for 30 min, allowing the formation of reactive NHS ester intermediates on the rGO surface. Following activation, the suspension was centrifuged and washed with 20 mmol L^{-1} PBS (pH 7.4) to remove excess EDC, NHS and reaction by-products. The activated rGO was subsequently redispersed in PBS containing 50 µg of mouse monoclonal anti-tau antibody, followed by incubation on an orbital shaker at 10 °C for 2 h to facilitate covalent attachment of the antibody through amide bond formation. To minimise non-specific adsorption during subsequent biosensing measurements, the remaining active surface sites were passivated using 2% (w/v) BSA prepared in PBS for 30 min. The functionalised material was then centrifuged at 16,000 × g for 10 min to remove unbound antibodies and excess blocking agent before being washed with PBS and stored at 4 °C until use. For electrochemical sensing experiments, recombinant Tau-441 (P301S) protein was prepared in PBS at a concentration of 0.2 µg mL^{-1}. This concentration was selected as the target analyte concentration for evaluating the response of the antibody-functionalised rGO-IDE sensing platform. The overall EDC/NHS functionalisation process is illustrated schematically in Figure 3, showing activation of carboxyl groups on rGO, antibody immobilisation, BSA blocking, and subsequent tau protein deposition.

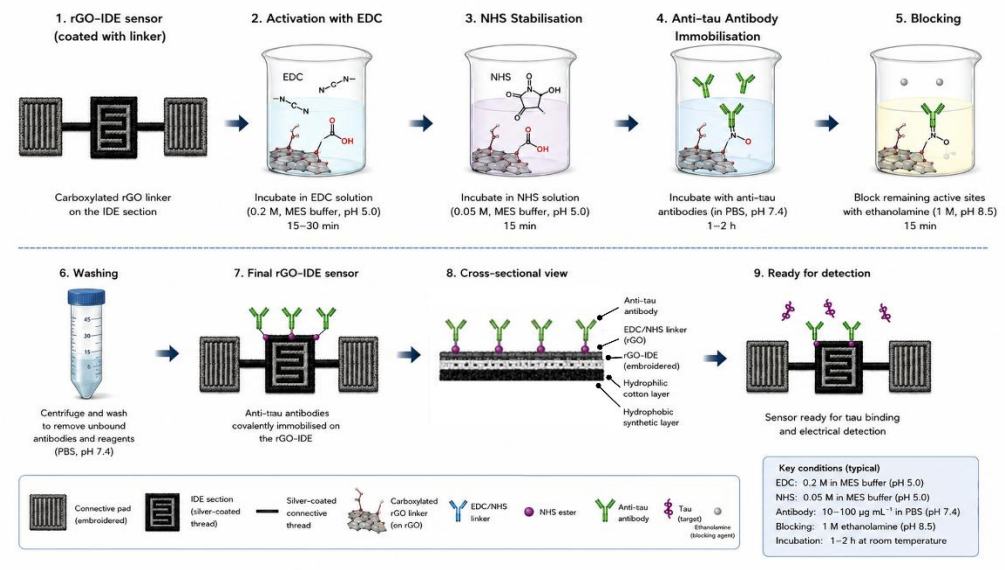


Fig 3. Schematic of the experiment method utilizing antibody-coated sensors

2.5 Electrical Measurements

Electrical resistance measurements were performed while droplets of water, phosphate buffered saline, artificial saliva, Aβ and Tau proteins were deposited onto the sensors.

Table 2. Electrical resistance metrics

Metric	Method used
Baseline resistance	Median resistance between 540–600 s (pre-droplet window)
Minimum resistance	Lowest resistance after 600 s
Time to minimum	Time (s) at which the minimum resistance occurs
Steady-state resistance	Median of the final ~10% of post-droplet measurements
ΔR	Steady-state resistance − baseline resistance
%ΔR	(ΔR / Baseline) × 100

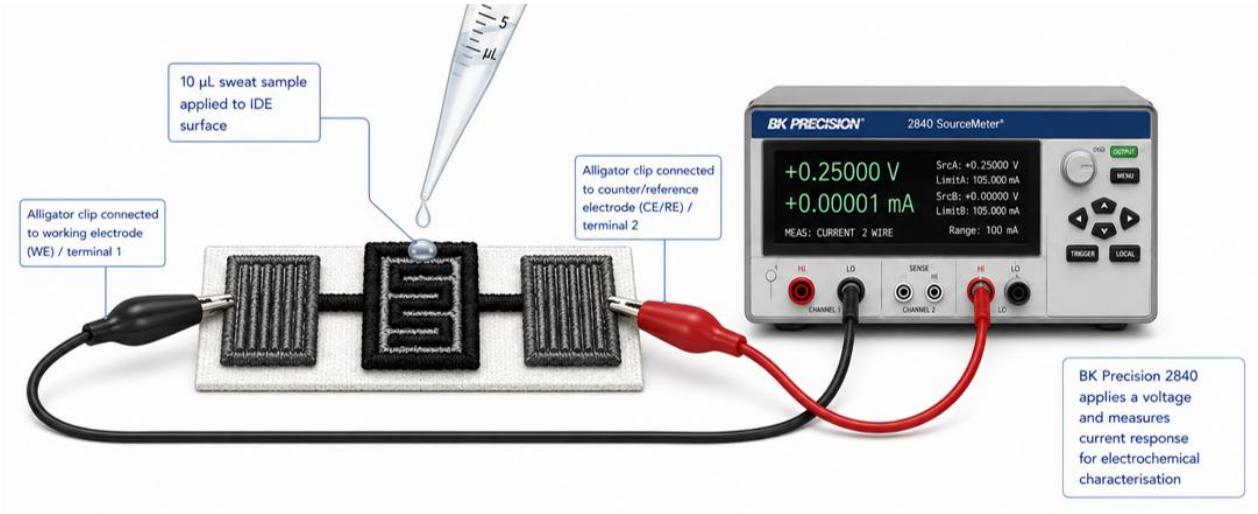


Fig 4. Schematic of the sensing platform electrical characterisation testing method

3. Results and Discussion

The performance of the fabricated textile biosensing platforms were evaluated through a combination of microstructural characterisation and electrical sensing experiments. The objective of this section was to determine how the graphene-based coatings influence sensor stability, wettability, and biomarker detection capability. While the present study demonstrates the feasibility of detecting Tau protein using AntiTau-functionalised textile biosensing platforms, quantitative analytical validation remains an important next step. Future work will investigate a range of Tau concentrations to establish calibration curves, determine sensor sensitivity, calculate the limit of detection (LOD) and limit of quantification (LOQ), and evaluate repeatability and reproducibility through statistical analysis of multiple independent sensor replicates.

3.1 Scanning Electron Microscope (SEM)

Scanning Electron Microscope (SEM) imaging indicated the coating of graphene materials onto the textile fibres. The SEM images presented (Fig 5. a – c) confirm that the graphene coatings were deposited onto the embroidered conductive fibres. In the GO-coated sensors (Fig 5. a), the graphene oxide flakes appear as thin layered structures covering the surface of the silver-coated threads. The flakes exhibit relatively consistent morphology across the sensing region, suggesting that the dropcasting process resulted in a reasonably uniform distribution of the graphene oxide material. The measured flake sizes range approximately between 700 µm and 1500 µm, indicating the presence of large conductive domains capable of forming electrical pathways across the electrode surface. A higher-magnification image (Fig. 5b) reveals that the graphene flakes adhere closely to the underlying textile fibres while still maintaining the fibrous morphology of the substrate. This is advantageous for textile biosensors, as the porous fibre structure allows interaction with liquid samples while the graphene coating provides electrical conductivity.

In comparison, the rGO-coated sensors (Fig 5. c) exhibit a slightly more compact surface morphology. This structural difference is consistent with the reduction process, in which oxygen-containing functional groups are removed from the GO structure. The resulting rGO material typically exhibits increased electrical conductivity and a more aggregated graphene network. The denser morphology observed in Fig 5. c suggests improved electrical contact between graphene domains, which may contribute to the improved electrical stability observed in later experiments.

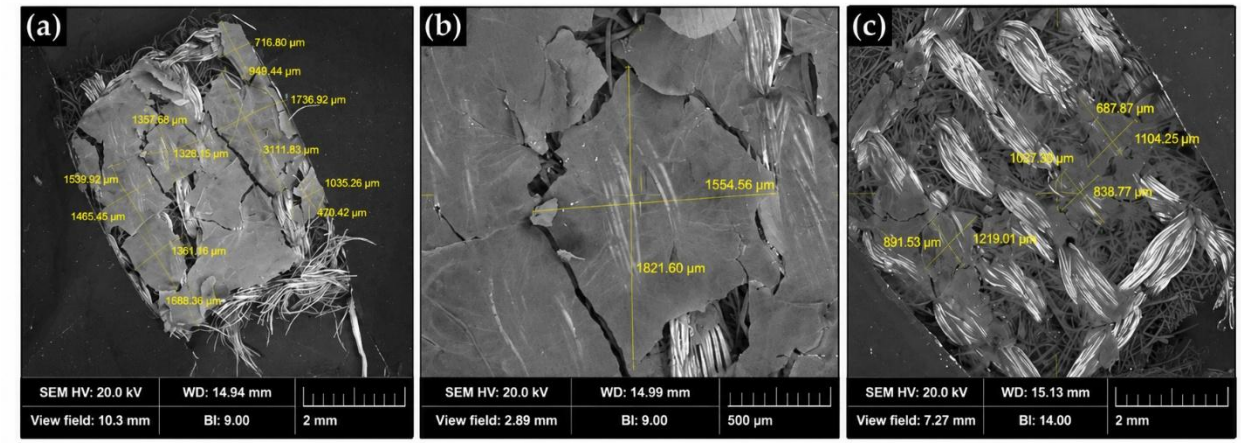


Figure 5. a) SEM images with graphite flake measurements b) GO-coated sample c) rGO-coated sensor with graphite flake measurements

3.2 Energy-dispersive X-ray spectroscopy (EDS)

Energy-dispersive X-ray spectroscopy was used to determine the elemental composition of the coated sensors and verified the presence of carbon-based graphene structures along with conductive silver threads. The elemental maps presented in Fig 6 confirm the presence of key elements associated with the functionalised substrate. Carbon and oxygen signals dominate the spectra, corresponding to the graphene-based coatings applied to the textile electrodes. The presence of these elements confirms the successful deposition of GO and rGO materials on the sensor surface. Silver signals are also clearly visible in the elemental maps, corresponding to the conductive embroidery thread used to form the interdigitated electrodes.

Minor trace elements, including potassium (0.73%), calcium (2.24%), and manganese (0.5%), were detected in small quantities. These elements are likely residues from the experimental testing phase, particularly from solutions such as phosphate buffered saline. Their presence does not significantly affect sensor operation but indicates that small amounts of test solutions remained on the sensor surface following measurements. Overall, the EDS results support that the graphene coatings are present and uniformly distributed across the textile electrodes while maintaining electrical connectivity through the silver thread structure.

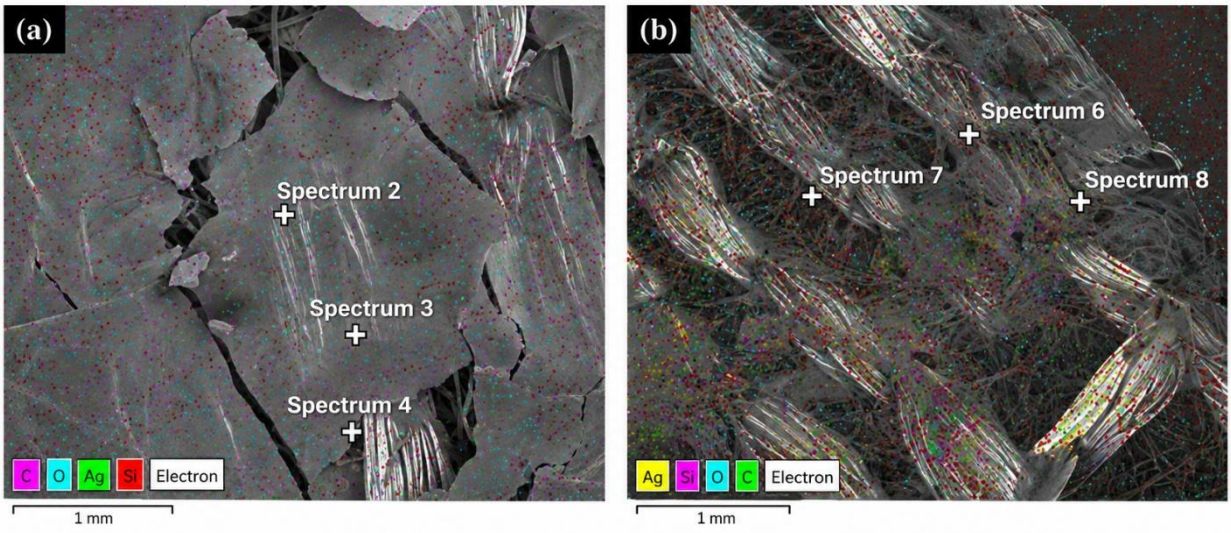


Fig 6. EDS elemental maps overlaid on SEM images a) GO sensor with three spectra locations highlighted b) rGO sensor with three spectra locations highlighted

3.3 Raman Spectroscopy

Raman spectroscopy was used to confirm the structural characteristics of the graphene materials used in the sensor coatings. The Raman spectrum shown in Fig. 7 displays two characteristic peaks corresponding to the D band and G band, which are commonly observed in graphene-based materials [25], [26]. The D band, observed at approximately 1351 cm^{-1}, is associated with structural defects or disorder within the graphene lattice. These defects may arise from the oxidation process used during graphene oxide synthesis or from functionalisation of the graphene surface. The presence of a pronounced D peak therefore indicates that the graphene material contains a significant number of defect sites.

The G band appears at approximately 1590 cm^{-1} and corresponds to the in-plane vibration of sp^2 hybridised carbon atoms. This peak is characteristic of graphitic materials and confirms the presence of conductive carbon structures within the coating [26]. The ratio of the D and G band intensities provides insight into the structural quality of the graphene material. In the AntiTau-rGO samples, a slightly higher D-band intensity was observed compared to the plain rGO sensors. This increase is likely due to the introduction of additional surface disorder caused by antibody conjugation. The presence of these functional groups is beneficial for biosensing applications, as defect sites can act as binding locations for biomolecules.

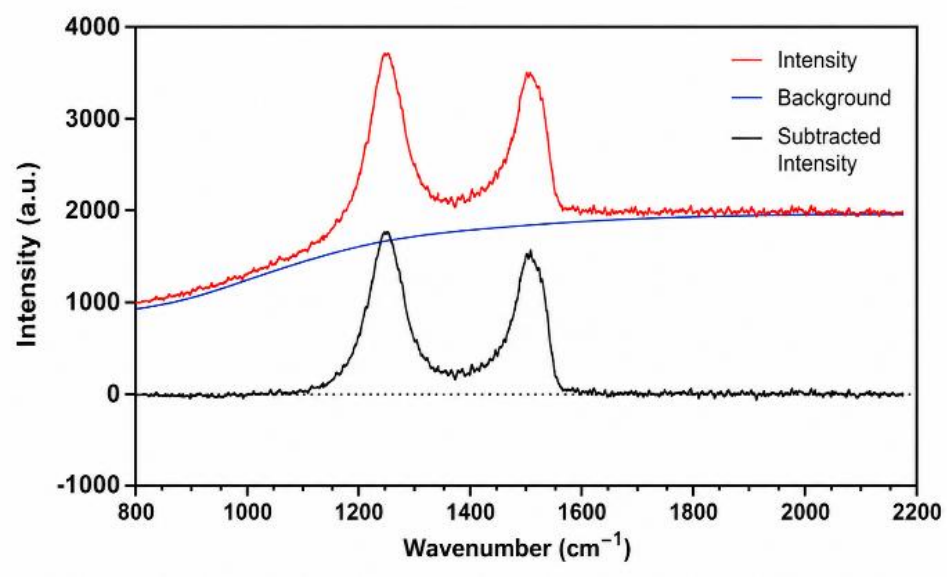


Fig 7. Raman spectrum maps of rGO sample

3.4 Contact angle analysis and surface wettability

The static water contact angle measurements for the untreated, GO-coated and rGO-coated textile substrates are presented in Fig. 8(a–f)**.** Contact angle analysis was performed to evaluate the influence of graphene functionalisation on the wettability of the embroidered sensing platform, as surface wetting plays a critical role in analyte transport, sample distribution and electrochemical sensing performance. The untreated textile substrates (Fig. 8(a) and (b)) exhibited contact angles of approximately 127.1° and 122.9°**,** respectively, confirming the inherently hydrophobic nature of the textile surface. The high contact angles indicate limited spreading of the water droplet, resulting in reduced interaction between the liquid sample and the sensing region.

Following deposition of the graphene oxide (GO) coating (Fig. 8(c) and (d)), the contact angle decreased to approximately 119.4° and 88.2°, demonstrating a significant increase in surface wettability. This behaviour is attributed to the presence of oxygen-containing functional groups, including hydroxyl, epoxy and carboxyl groups, which increase the surface polarity and enhance the interaction between the aqueous droplet and the graphene coating. Improved wettability facilitates greater contact between the sample and the sensing surface, promoting more effective analyte transport to the electrode interface. The reduced graphene oxide (rGO)-coated substrates (Fig. 8(e) and (f)) exhibited contact angles of approximately 97.1**°** and 88.2**°**, indicating further modification of the wetting behaviour following chemical reduction. Although reduction removes a proportion of the oxygen-containing functional groups present on GO, the apparent wettability is also governed by the morphology of the graphene coating, fibre roughness and capillary effects associated with the porous textile structure. These combined effects resulted in efficient spreading of the liquid across the embroidered sensing region while maintaining droplet localisation over the interdigitated electrodes.

Overall, the contact angle measurements demonstrate that graphene surface modification significantly influences the wetting characteristics of the textile substrate. Compared with the untreated textile, both GO and rGO coatings reduced the water

contact angle, thereby improving liquid–surface interaction. The enhanced wettability is expected to facilitate more uniform sample distribution and increase the effective contact area between the target analyte and the antibody-functionalised sensing surface, contributing to improved measurement repeatability and electrochemical sensing performance.

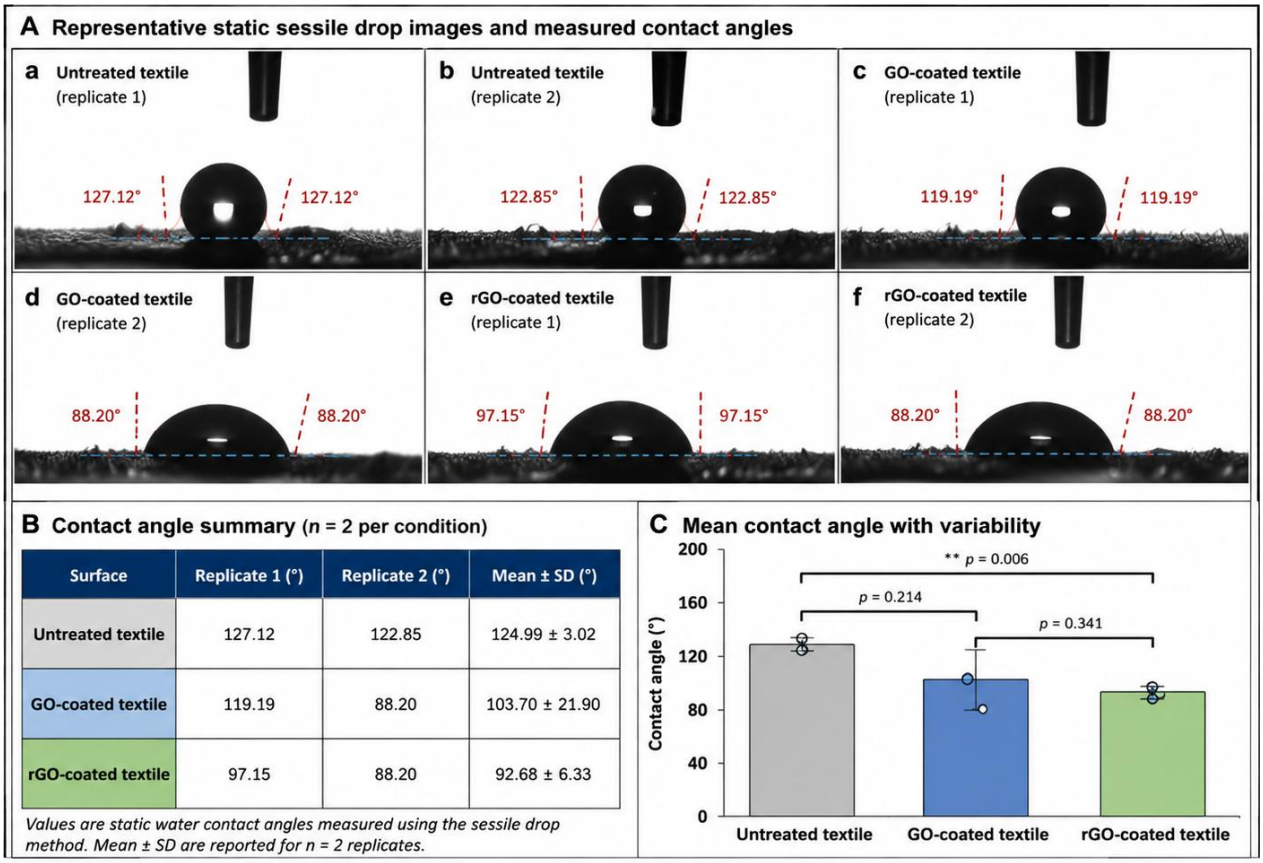


Fig 8. Wettability analysis of textile sensor surface A) Representative static sessile drop images with measures contact angles for untreated textile (a.b) GO-coated textile (c, d) and rGO-coated textile (e, f). B) Summary of contact angle values (mean ± SD) for each surface (n = 2). C) Mean contact angle comparison with SD.

3.5 Electrical response of GO-coated sensors

The electrical behaviour of the GO-coated sensors is shown in Fig 9. When droplets of water, phosphate buffered saline, artificial saliva, or Aβ protein are deposited onto the sensor surface at approximately 60 seconds, a significant drop in resistance is observed. This drop in resistance occurs because the added liquid creates a conductive pathway between the electrode fingers of the interdigitated structure. As the liquid spreads across the graphene-coated region, it effectively reduces the electrical resistance measured between the electrodes. However, a notable feature of the GO sensor results is the high variability between repeated experimental runs. The magnitude of resistance change varies by nearly an order of magnitude in some cases. This variability can be attributed to the strong hydrophilic nature of the GO surface, which allows the liquid droplet to spread rapidly and unevenly across the textile substrate. As a result, the GO-coated

sensors are highly sensitive to the presence of liquids but lack sufficient stability for reliable biomarker detection.

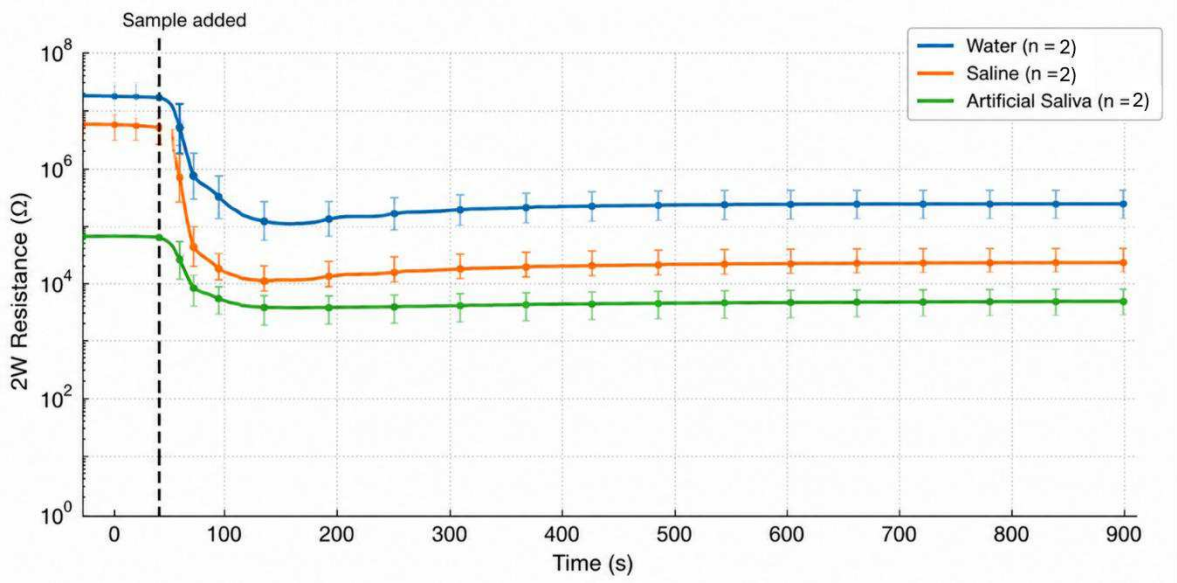


Fig 9. Mean (± SD) two-wire resistance of GO-coated embroidered sensors exposed to difference solutions over 900 s. The dashed line at 60 s indicates the time of droplet addition

3.6 Electrical response of rGO-coated sensors

The electrical behaviour of the rGO-coated sensors is presented in Figure 10. Compared with the GO sensors, the rGO-coated devices exhibit significantly smaller fluctuations in resistance when exposed to the same test solutions. This improved stability can be attributed to several factors. First, the reduction of oxygen functional groups in rGO decreases the hydrophilicity of the graphene surface, resulting in slower liquid absorption. Second, the increased electrical conductivity of rGO provides a more stable baseline resistance. Although rGO sensors demonstrate improved stability, the resistance changes observed following exposure to Aβ are relatively small and inconsistent.

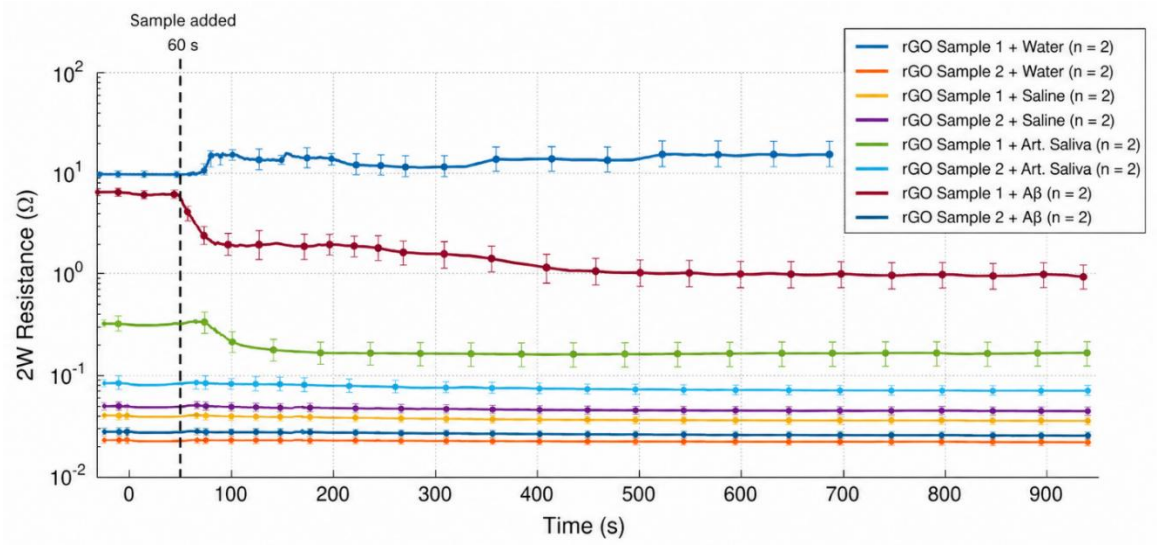


Fig 10. Mean (± SD) two-wire resistance of rGO sensor Samples 1 and 2 upon addition of water, phosphate buffered saline, artificial saliva and Aβ (n=2 independent sensors). The dashed line at 60 s indicates the time of droplet addition

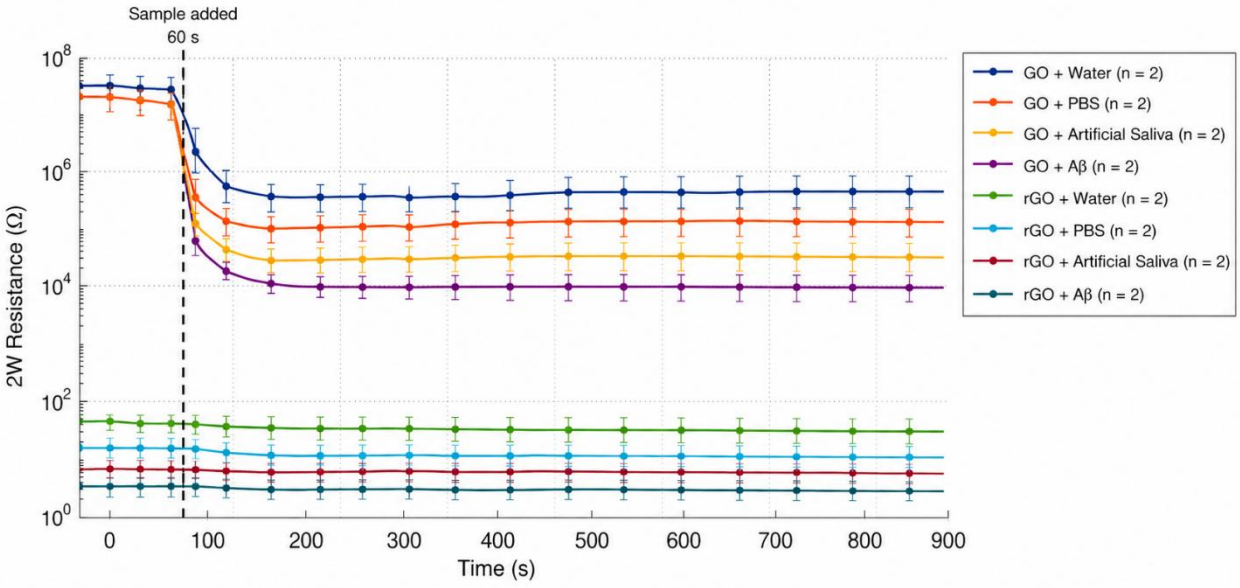


Fig 11. Mean (± SD) two-wire resistance of GO-coated embroidered sensors (samples 1 and 2) upon addition of water, phosphate buffered saline, artificial saliva and Aβ (n = 2 independent sensors).

3.7 AntiTau-GO Samples A and AntiTau-rGO Sample B

Figure 12 compares the electrical responses of the AntiTau-functionalised GO and AntiTau-functionalised rGO embroidered biosensing platforms following exposure to water, artificial saliva, Aβ and tau protein. All sensors exhibited a rapid reduction in resistance immediately following droplet application at 60 s before reaching a stable equilibrium. The AntiTau-rGO biosensing platforms demonstrated the largest resistance change following exposure to tau protein, whereas comparatively smaller responses

were observed for water, artificial saliva and Aβ. This behaviour indicates partial immobilisation of the anti-tau antibodies and potential interaction with the target biomarker. In contrast, the AntiTau-GO sensors exhibited greater baseline drift and increased variability between measurements, consistent with the lower electrical stability previously observed for GO coatings. The enhanced performance of the AntiTau-rGO biosensors is attributed to the improved electrical conductivity of the reduced graphene oxide coating together with the stable covalent attachment of antibodies through EDC/NHS coupling chemistry, providing a more reproducible sensing interface for electrochemical detection.

At time t = 0 s, all test runs show an initial resistance of 10^7 to 10^8 Ω. This is consistent with a dry sensor, or a sensor without a conductive medium present, as is expected for GO-coated sensors in baseline conditions. At approximately 60 seconds, there is a sharp and substantial drop in resistance in all tests, which validates that water was added to the sensor surface at that point. This drop in resistance reflects the sensor's response to the conductive nature of the water, which lowers the resistance by creating a conductive path on the GO-coated surface. The 5 test runs remain at a lower resistance compared to the start of the test, between 10^4 and 10^6 Ω.

Secondly, the stability of AntiTau-GO Sample A when artificial saliva was added to the surface is investigated. At 60 seconds a 0.1 mL droplet of artificial saliva is added to the surface at which point all 5 runs show a sharp decrease in resistance. The remaining time of all 5 test runs shows the resistance stays between 10^4 Ω to 10^5 Ω. Thirdly, when 0.1 mL of Tau protein is dropped onto the surface at time t = 0 seconds, all 5 test runs start at a high resistance value in similar behaviour to the previous graphs. At 60 seconds, when the 0.1 mL of Tau protein is added to the surface, all 5 test runs show a sharp decrease in the resistance, but to different levels of magnitude. The decrease in resistance in this instance ranges between 10^4 and 10^7 Ω suggesting a more complex interaction between Tau and the GO-coated surface.

Finally, the resistance results of the AntiTau-GO Sample A when Aβ protein is added to the surface as a 0.1 mL droplet are displayed. This test was to compare the results of the sensor with a different, non-target, biomarker protein for AD. The starting resistance, at time t = 0 seconds, is between 106 and 108 Ω, consistent with the previous tests. When 0.1 mL of Aβ protein is added, at 60 seconds, there is a comparatively small drop in the resistance of the sample across all 5 test runs. The results in this experiment show more fluctuations over time compared to when water, artificial saliva, and Tau were added to the sensor surface. This could be due to the Aβ protein aggregating on the sensor surface, or its binding sites interacting differently to the Tau protein, as Aβ is not the target molecule for AntiTau antibody. Therefore the AntiTau coating displays some response to the Aβ protein but a much less stable result when compared with the target protein Tau. AntiTau-functionalised sensors showed improved readout response for Tau protein compared with Aβ, suggesting some degree of recognition on the sensor.

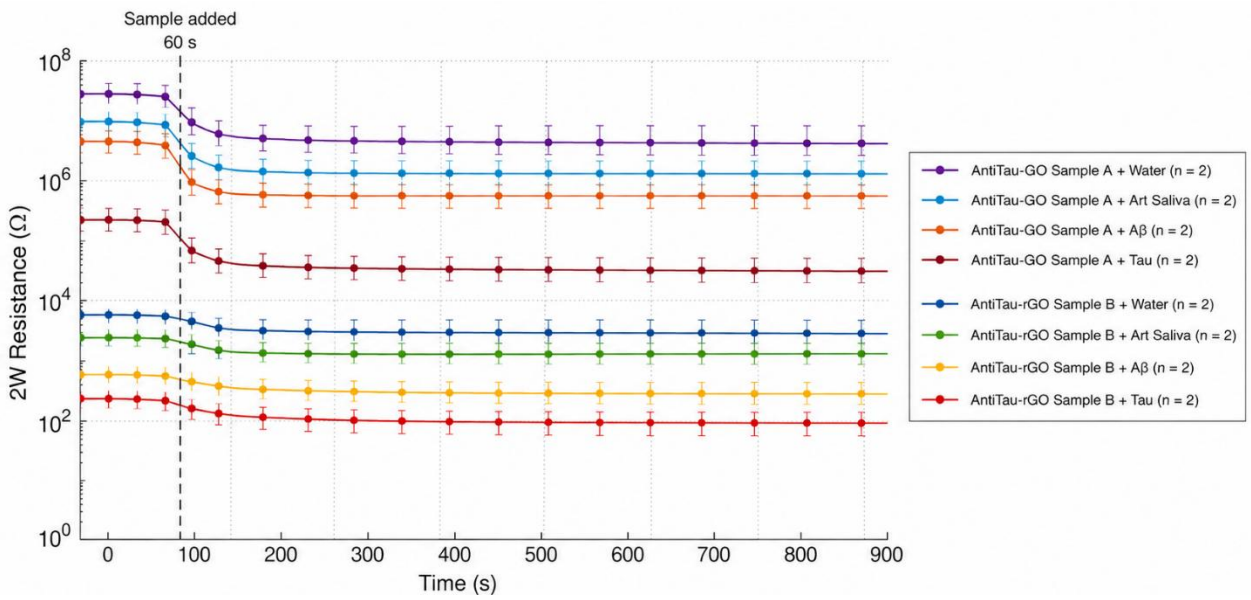


Fig 12. Mean (± SD) two-wire resistance of AntiTau-functionalised GO (Sample A) and AntiTau-rGO (Sample B) embroidered sensors following exposure to water, Aβ, and tau protein (n = 2 independent sensors). Resistance was monitored for 900s, with sample addition at 60 s.

4. Conclusion

This study evaluated the feasibility of producing graphene□based textile biosensing platforms for detecting Alzheimer's Disease biomarkers in saliva, based on an assessment of their stability. rGO coatings improved electrical stability while AntiTau functionalisation demonstrated some degree of recognition for Tau protein. This work suggests that the performance of textile-based biosensing platforms are governed by the interplay between graphene material properties and biochemical functionalisation. While GO-coated sensors exhibit high sensitivity, their strong hydrophilicity leads to significant signal variability and poor reproducibility. In contrast, rGO coatings provide enhanced electrical stability and more consistent resistance responses due to improved conductivity and controlled wettability. The incorporation of AntiTau antibodies suggested some differentiation from Aβ responses. Among all configurations, the AntiTau-rGO sensors deliver the best overall performance, achieving a more stable output. Furthermore, the reproducible resistance–time signatures obtained from AntiTau-rGO sensors provide a strong foundation for integration with machine learning algorithms, supporting the development of wearable, non-invasive diagnostic systems for early Alzheimer's disease detection. Future studies will focus on quantitative analytical validation, including concentration-dependent calibration, determination of analytical sensitivity and LOD, statistical evaluation of repeatability and reproducibility, and testing with clinical saliva samples to assess diagnostic performance.

5. References

[1] World Health Organization, *Global action plan on the public health response to dementia 2017–2025*. Geneva: World Health Organization, 2017. Accessed: Jan. 29, 2024. [Online]. Available: https://iris.who.int/handle/10665/259615

[2] E. Nichols *et al.*, ‘Estimation of the global prevalence of dementia in 2019 and forecasted prevalence in 2050: an analysis for the Global Burden of Disease Study 2019’, *The Lancet Public Health*, vol. 7, no. 2, pp. e105–e125, Feb. 2022, doi: 10.1016/S2468-2667(21)00249-8.
[3] T. T. Htike, S. Mishra, S. Kumar, P. Padmanabhan, and B. Gulyás, ‘Peripheral Biomarkers for Early Detection of Alzheimer’s and Parkinson’s Diseases’, *Mol Neurobiol*, vol. 56, no. 3, pp. 2256–2277, Mar. 2019, doi: 10.1007/s12035-018-1151-4.
[4] J. Hardy and D. J. Selkoe, ‘The Amyloid Hypothesis of Alzheimer’s Disease: Progress and Problems on the Road to Therapeutics’, *Science*, vol. 297, no. 5580, pp. 353–356, Jul. 2002, doi: 10.1126/science.1072994.
[5] C. R. Jack *et al.*, ‘A/T/N: An unbiased descriptive classification scheme for Alzheimer disease biomarkers’, *Neurology*, vol. 87, no. 5, pp. 539–547, Aug. 2016, doi: 10.1212/WNL.0000000000002923.
[6] S. Palmqvist *et al.*, ‘Performance of Fully Automated Plasma Assays as Screening Tests for Alzheimer Disease–Related β-Amyloid Status’, *JAMA Neurol*, vol. 76, no. 9, p. 1060, Sep. 2019, doi: 10.1001/jamaneurol.2019.1632.
[7] S. Lehmann *et al.*, ‘Comparative performance of plasma pTau181/Aβ42, pTau217/Aβ42 ratios, and individual measurements in detecting brain amyloidosis’, *eBioMedicine*, vol. 117, p. 105805, Jul. 2025, doi: 10.1016/j.ebiom.2025.105805.
[8] ‘FDA Clears First Blood Test Used in Diagnosing Alzheimer’s Disease | FDA’. Accessed: Jul. 13, 2026. [Online]. Available: https://www.fda.gov/news-events/press-announcements/fda-clears-first-blood-test-used-diagnosing-alzheimers-disease
[9] N. J. Ashton *et al.*, ‘Diagnostic Accuracy of a Plasma Phosphorylated Tau 217 Immunoassay for Alzheimer Disease Pathology’, *JAMA Neurol*, Jan. 2024, doi: 10.1001/jamaneurol.2023.5319.
[10] M. Shi *et al.*, ‘Salivary Tau Species are Potential Biomarkers of Alzheimer’s Disease’, *JAD*, vol. 27, no. 2, pp. 299–305, Nov. 2011, doi: 10.3233/JAD-2011-110731.
[11] D. Shahdeo *et al.*, ‘Label free detection of SARS CoV-2 Receptor Binding Domain (RBD) protein by fabrication of gold nanorods deposited on electrochemical immunosensor (GDEI)’, *Biosensors and Bioelectronics*, vol. 212, p. 114406, Sep. 2022, doi: 10.1016/j.bios.2022.114406.
[12] A. J. Bandodkar and J. Wang, ‘Non-invasive wearable electrochemical sensors: a review’, *Trends in Biotechnology*, vol. 32, no. 7, pp. 363–371, Jul. 2014, doi: 10.1016/j.tibtech.2014.04.005.
[13] D. A. C. Brownson and C. E. Banks, ‘Introduction to Graphene’, in *The Handbook of Graphene Electrochemistry*, London: Springer London, 2014, pp. 1–22. doi: 10.1007/978-1-4471-6428-9_1.
[14] B. Pegu, S. Devi, D. J. Sonowal, R. Boruah, and S. Konwer, ‘A comparative study on the synthesis of highly conductive reduced graphene oxide from GO using various green reductant for methanol sensors’, *J Mater Sci: Mater Electron*, vol. 35, no. 19, p. 1340, Jul. 2024, doi: 10.1007/s10854-024-13055-9.
[15] G. T. Hermanson, *Bioconjugate techniques*, 3d edition. Amsterdam: Academic Press, 2013.
[16] D. C. Marcano *et al.*, ‘Improved Synthesis of Graphene Oxide’, *ACS Nano*, vol. 4, no. 8, pp. 4806–4814, Aug. 2010, doi: 10.1021/nn1006368.
[17] W. Zhao *et al.*, ‘Sensitivity-Enhancing Strategies of Graphene Field-Effect Transistor Biosensors for Biomarker Detection’, *ACS Sens.*, vol. 9, no. 6, pp. 2705–2727, Jun. 2024, doi: 10.1021/acssensors.4c00322.
[18] T. Chudziak *et al.*, ‘A comparative investigation of the chemical reduction of graphene oxide for electrical engineering applications’, *Nanoscale*, vol. 15, no. 44, pp. 17765–17775, 2023, doi: 10.1039/D3NR04521H.

[19] O. Zolti, B. Suganthan, and R. P. Ramasamy, ‘Lab-on-a-Chip Electrochemical Biosensors for Foodborne Pathogen Detection: A Review of Common Standards and Recent Progress’, *Biosensors*, vol. 13, no. 2, p. 215, Feb. 2023, doi: 10.3390/bios13020215.
[20] G. Kwame Fobiri, B. Eghan, R. Kanyire Seidu, and B. Tawiah, ‘A review of functionalized graphene-oxide in wearable textile sensors and supercapacitors for biomedical applications’, *Essential Chem*, vol. 2, no. 1, p. 2493111, Dec. 2025, doi: 10.1080/28378083.2025.2493111.
[21] World Health Organization, *Global strategy on digital health 2020-2025*. World Health Organization, 2021. Accessed: Sep. 11, 2023. [Online]. Available: https://apps.who.int/iris/handle/10665/344249
[22] G. Sun, ‘Disposable and reusable medical textiles’, in *Textiles for Hygiene and Infection Control*, Elsevier, 2011, pp. 125–135. doi: 10.1533/9780857093707.2.125.
[23] K. R. Ratinac, W. Yang, S. P. Ringer, and F. Braet, ‘Toward Ubiquitous Environmental Gas Sensors—Capitalizing on the Promise of Graphene’, *Environ. Sci. Technol.*, vol. 44, no. 4, pp. 1167–1176, Feb. 2010, doi: 10.1021/es902659d.
[24] Z. Grabarek and J. Gergely, ‘Zero-length crosslinking procedure with the use of active esters’, *Analytical Biochemistry*, vol. 185, no. 1, pp. 131–135, Feb. 1990, doi: 10.1016/0003-2697(90)90267-D.
[25] K. N. Kudin, B. Ozbas, H. C. Schniepp, R. K. Prud’homme, I. A. Aksay, and R. Car, ‘Raman Spectra of Graphite Oxide and Functionalized Graphene Sheets’, *Nano Lett.*, vol. 8, no. 1, pp. 36–41, Jan. 2008, doi: 10.1021/nl071822y.
[26] R. Muzyka, S. Drewniak, T. Pustelny, M. Chrubasik, and G. Gryglewicz, ‘Characterization of Graphite Oxide and Reduced Graphene Oxide Obtained from Different Graphite Precursors and Oxidized by Different Methods Using Raman Spectroscopy’, *Materials*, vol. 11, no. 7, p. 1050, Jun. 2018, doi: 10.3390/ma11071050.